Novel tools and observables for jet physics in heavy-ion collisions

Harry Arthur Andrews[bir], Liliana Apolinario[lip,ist], Redmer Alexander Bertens[ten], Christian Bierlich[lund,bohr], Michal Deak[ifj], David d'Enterria[cern], Krzysztof Kutak[ifj], Chang Ning-Bo[itp], Dennis Perepelitsa[col], Gavin Salam*[cern], Martin Spousta[char], José Guilherme Milhano[lip,ist,cern], Konrad Tywoniuk[cern], Urs A. Wiedemann[cern], and Korinna C. Zapp[lip,cern]

[bir] *University of Birmingham, Birmingham B15 2TT, United Kingdom*
[lip] *LIP, Av. Prof. Gama Pinto, 2, P-1649-003 Lisboa , Portugal*
[ist] *Instituto Superior Técnico (IST), Universidade de Lisboa, Av. Rovisco Pais 1, 1049-001, Lisbon, Portugal*
[ten] *University of Tennessee, Knoxville, TN, USA-37996*
[lund] *Dept. of Astronomy and Theoretical Physics, S olvegatan 14A, S-223 62 Lund, Sweden*
[bohr] *Niels Bohr Institute, Blegdamsvej 17, 2100 Copenhagen, Denmark*
[ifj] *Instytut Fizyki Jądrowej (PAN), ul. Radzikowskiego 152, 31-342 Kraków, Poland*
[cern] *Theoretical Physics Department, CERN, 1211 Geneva 23, Switzerland*
[itp] *Institute of Theoretical Physics, Xinyang Normal University, Xinyang, Henan 464000, China*
[col] *University of Colorado Boulder, Boulder, CO 80309, USA*
[char] *Charles University, V Holesovickach 2, 180 00 Prague, Czech Republic*

June 13, 2018

Abstract

Studies of fully reconstructed QCD jets in heavy-ion collisions remain one of the most firmly established programs aimed at extracting properties of hot and dense nuclear matter. Most recently, substructure observables have opened new and exciting directions by introducing techniques amenable to dissecting jets and extending the plethora of established observables. This report, summarizing the main lines of discussion at the 5th Heavy Ion Jet Workshop and CERN TH institute "Novel tools and observables for jet physics in heavy-ion collisions" in 2017, presents a first attempt at outlining a strategy for isolating and identifying the relevant physical processes that are responsible for the observed modifications by combining theory insights with sophisticated jet reconstruction techniques, including grooming and background subtraction algorithms.

CERN-TH-2018-xxx, LU-TP 18-14, IFJPAN-IV-2018-8, MCNET-18-xx

1 Introduction

In recent years, observables involving fully reconstructed jets, produced in heavy-ion collisions, have been established as important tools to probe the properties of the underlying hot and dense QCD medium. From a reciprocal point of view, they also shed light on the details of parton fragmentation and hadronisation in the presence of final-state interactions. These developments are mainly driven by a dedicated experimental effort that aim at fully exploit the detector capabilities and experimental techniques at current high-energy colliders. On the theory side, an enhanced level of sophistication of the modeling of both jet fragmentation and its coupling to the medium evolution, often implemented as Monte-Carlo parton showers or event generators, allow to scrutinize the details of jet-medium interactions using a wide range of high-p_{T} processes.

Jets are excellent probes of the quark-gluon plasma (QGP) for several reasons; here we briefly outline but a few. Firstly, since they are multi-parton objects containing color degrees of freedom they are affected by final-state interactions with a deconfined medium. Secondly, in course of their evolution jets

*On leave from CNRS, UMR 7589, LPTHE, F-75005, Paris, France and from Rudolf Peierls Centre for Theoretical Physics, 1 Keble Road, Oxford OX1 3NP, UK.

can probe various length scales of the QGP, providing a complementary window with regard to bulk observables that are dominated by soft physics.

The way in which high-p_{T} observables in heavy-ion collisions deviate from baseline measurements in proton-proton collisions is generically referred to as "jet quenching". This term arose historically in connection with the first data on the suppression on high-p_{T} hadron suppression and related di-jet/photon-jet asymmetries measured at RHIC. These processes clearly involve a large variety of scales, ranging from the jet scale to thermal scales of the QGP, as will also be explained in more detail below. Typical jet quenching observables will therefore be sensitive to perturbative and non-perturbative contributions in varying degree. This can complicate the interpretation of the considered observables and obfuscate the extraction of information about the underlying medium. Besides, additional background subtraction algorithms have to be applied in the more noisy heavy-ion environment, complicating the procedure of statistically removing detector effects (unfolding). Therefore a joint community effort between theory and experiment is crucial to fully take advantage of the potential of these QGP probes.

Many of these complications are less pressing or absent when measuring single-hadron spectra or hadron correlations. Hence, one notable example of such an joint effort was the so-called "brick problem" [1, 2], organized by the TECHQM collaboration [**?**], which aimed at clarify differences and similarities between various theoretical implementations of jet quenching on the level of single-hadron spectra in heavy-ion collisions. The simplification allowing for such a comprehensive comparison was to reduce the complexity of the modeling of the underlying medium to a static, one-dimensional "brick" with constant density. Based on this exercise, it resulted in a comprehensive effort to estimate the jet quenching parameter $\hat{q}$ along with its uncertainties [2].

The joint organization of the 5th Heavy Ion Workshop and CERN TH institute "Novel tools and observables for jet physics in heavy-ion collisions" took place at CERN 25 August – 1 September 2017 [3]. The main objective of the meeting was to bring together experimentalists and theorists in order to identify relevant jet observables that are sensitive to different aspects of the final-state interactions with the dense medium created in heavy-ion collisions and study the added potential of jet substructure techniques in this context.

Due to the high level of complexity related to the experimental determination and theoretical treatment of jet observables, a comprehensive effort of comparing models against each other and against data on a wide range of observables is out of scope and, probably, would not allow to draw meaningful conclusions. Instead, the workshop provided an opportunity to consider jet observables in heavy-ion collisions from a new perspective to a large extent made available through novel substructure techniques. This report sums up the main discussions that took place during the meeting, and presents a selected number of numerical studies using existing tools. These mainly include the Monte Carlo (MC) event generators PYTHIA 8 [4] for simulating the proton-proton baseline, and in-medium jet evolution codes QPYTHIA [5] and JEWEL [6, 7]. We refer the interested reader to Appendix A for further details on the MC's utilized in the studies presented below. The selected parton shower MC's were used for sake of convenience, and we look forward to extend the suite of studied generators, including MARTINI [**?**, **?**], HYDJET++ [**?**], YaJEM [**?**] and MATTER [**?**] as well as newly developed codes, most notably JETSCAPE [**?**], in future editions of the workshop. In addition, for jet reconstruction we made extensive use of FastJet [**?**, **?**] and for the purposes of additional pile-up mitigation in heavy-ion context, we studied constituent subtraction (CS) [10] and SoftKiller (SK) [11].

We organize the report according to two main motifs. In the first part, Section 2, we introduce for the first time, in the context of heavy-ion studies, the concept of a splitting map, based on the Lund kinematical diagram [8]. Filling this map gives a operational representation of the radiation pattern implemented in a given showering algorithm. It also provides a direct, visual impression of what phase space region is being most significantly modified by medium effects. In detail,

Section 2.1 gives a brief introduction to theoretical concepts that are useful for understanding the Lund diagram on the level of a single splitting, both for vacuum showers and showers in the medium.

Section 2.2 describes in detail the procedure to fill the splitting map, by describing the steps related to jet reclustering and calculation of the variables that go into the map. In particular, we study the impact of changing the reclustering algorithm, giving rise to different jet "histories" on the level of the PYTHIA vacuum shower.

Section 2.3 presents a study of the splitting maps of in-medium MC parton showers, QPYTHIA and JEWEL. Finally, in Section 2.3.1, we study the resilience of the observed features at generator level to uncorrelated background by embedding the jet samples into a realistic heavy-ion environment.

While the splitting maps contain the maximal amount of information, since they accumulate the kinematics of every splitting, they are also amenable to more exclusive examinations for instance through the implementation of jet "tagging" and "grooming" procedures. These tools are extensively used in the high-energy community [**?**] for a wide range of purposes, spanning jet substructure studies and leveraging this control for studies of observables beyond pure QCD, see e.g. [26, **?**] for the most recent reviews. They have also been previously applied in Monte-Carlo studies for heavy-ion collisions [**?**, **?**, 21]. In studying concrete observables, we have mainly focussed on applying the so-called Soft Drop (SD) grooming procedure [9], to be detailed below, that aims at identifying the first hard jet branching. Hence, in the second part of the report, Section 3, we perform a set of MC studies, on generator level and including embedding into a realistic heavy-ion background, using state-of-the-art grooming techniques. These observables are however, not limited to substructure but are also used in order to extract more differential aspects from inclusive jet observables. In detail,

Section 3.1 presents the result for the groomed momentum-fraction z_g, subjet angle ΔR_{12} and the groomed mass M_g for QPYTHIA and JEWEL using three grooming settings (in this section, the studies were performed on generator level). We shed more light on the robustness of these results by checking the size of hadronization effects in the z_g distribution for three different SD settings Section 3.1.1. As in Section 2.2, we also perform a brief study on how the reclustering algorithms modify the distributions.

Section 3.2 suggests a complementary look on substructure by submitting the jet sample that goes in to constructing a fully inclusive observable to an additional grooming step. Concretely, we propose to "dissect" the jet sample using SD grooming and bin the data in terms of the angular separation of the hardest subjets, ΔR_{12}. We demonstrate this procedure on QPYTHIA and JEWEL samples for the nuclear modification factor R_{AA} and the photon-jet imbalance.

Finally, we wrap up with an outlook in Section 4.

2 Mapping the splittings of in-medium jets

2.1 Theoretical considerations

Jets are multi-particle observables and are experimentally accessed by assembling measured tracks and calorimeter energy deposition, or a combination of both, according to a jet algorithm. In the context of perturbative QCD, multiple splittings inside the jet cone have to be taken into account due to the mass singularity of QCD. In the medium, these splittings happen concurrently with, and are affected by, final-state interactions with the surrounding medium. It is therefore worth considering how medium scales, related to the medium size[1] and the local properties, will have an impact on the phase space of jet observables.

In this context, it is very useful to introduce the Lund kinematical diagram [8] for an arbitrary $1 \to 2$ splitting process. In the soft and collinear limit, and in the absence of medium interactions, the differential probability $\mathrm{d}P$ of emission of a gluon is given in terms of its kinematical variables by [17, 18]

$$\mathrm{d}P = 2\frac{\alpha_s C_i}{\pi}\,\mathrm{d}\log z\theta\,\mathrm{d}\log\frac{1}{\theta}\,, \tag{1}$$

where z and θ are the momentum fraction and angle, respectively, of the gluon that is emitted off a projectile parton in arbitrary color representation ($C_i = C_F$ for quark and $C_i = N_c$ for gluon splitting, respectively). Hence, for fixed coupling, the area spanned below the line $z = 1$, see Figure 1, is uniformly populated by emissions with weight $2\alpha_s C_i/\pi$. The radiation can take place up to the jet opening angle R. In this figure we have also explicitly mapped out the regimes of soft, large-angle and hard, collinear radiation. For future reference, it is worth keeping in mind that lines at fixed transverse momentum are horizontal, lines at fixed angle vertical, lines at fixed mass diagonal with a positive unit slope, and lines at fixed energy diagonal with a negative unit slope in this diagram.

Before discussing any additional elastic or inelastic processes arising by the presence of a medium, one could consider the fate of vacuum emissions given a certain medium size. It can most naively be compared with the time it takes for a original parton to split into two daughter partons of invariant mass

$$M^2 = z(1-z)p_{\mathrm{T}}^2\theta^2\,, \tag{2}$$

[1] For simplicity, in this section we treat the medium as static, where all jets traverse the same length L.

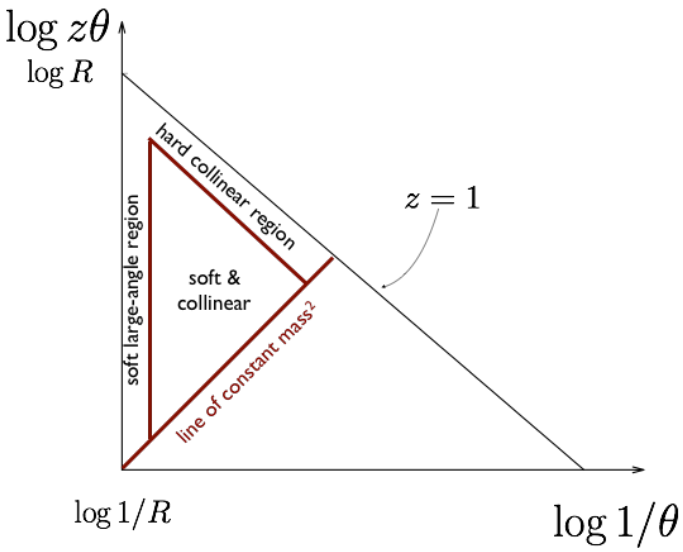

Figure 1: Lund kinematical diagram for vacuum radiation. Figure adapted from Ref. [25].

for small angles θ, where p_{T} is the longitudinal momentum of the parent parton, see Eq. (1). This time is the so-called *formation time*, and is related to the uncertainty of the time-scale of splitting $t_{\mathrm{f}} \sim \Delta E^{-1}$, and is explicitly given by

$$t_{\mathrm{f}} = \frac{2z(1-z)p_{\mathrm{T}}}{k_\perp^2} = \frac{2p_{\mathrm{T}}}{M^2}\,, \tag{3}$$

where $k_\perp = z(1-z)p_{\mathrm{T}}\theta$, in the small angle limit, is the relative transverse momentum of the splitting. This formula can easily be understood as the time-scale for decaying in the rest frame of the parent times its boost factor $\sim (1/M) \times (p_{\mathrm{T}}/M)$. In the following, we will only consider soft radiation and neglect and additional numerical factors to write $t_{\mathrm{f}} \sim (zp_{\mathrm{T}}\theta^2)^{-1}$.

Coming back to the diagram, let us identify emissions that happened inside the medium or, in other words, formation times that are shorter than the medium length ($t_{\mathrm{f}} < L$). This condition results in an area on the Lund diagram delimited by the line solving $t_{\mathrm{f}} = L$,

$$\log z\theta = \log\frac{1}{\theta} + \log\frac{1}{p_{\mathrm{T}}L}\,, \tag{4}$$

which is also represented in Figure 2. Hence, the area above the line marked $t_{\mathrm{f}} = L$ correspond to (vacuum) emissions that occur inside the medium. Emissions with $t_{\mathrm{f}} > L$ occupy the region below the line.

In order to proceed, we will have to assume something about how the jet constituents interact with the medium. For illustrative purposes we will assume that all propagating particles experience diffusive momentum broadening, where the amount of accumulated momentum is characterized by the dispersion $\langle k_\perp^2 \rangle = \hat{q}t$, t determining the time of in-medium propagation. The jet transport coefficient $\hat{q}$ acts as a diffusion constant in transverse space for the hard modes.[2]

Having this picture in mind, a second time-scale immediately becomes relevant. It is typically referred to as the decoherence time, since it gauges whether medium interactions resolve a particular splitting. This occurs whenever the size of the pair, which can be estimated as $x_\perp \sim \theta t$ for small angles, becomes comparable to the medium resolution scale $\lambda_\perp \sim (\hat{q}t)^{-1/2}$ which in turn is inverse to the transverse momentum accumulated by multiple scattering. By equating the two, $x_\perp \sim \lambda_\perp$, we find the parametric estimate for the decoherence time which turns out to be

$$t_{\mathrm{d}} = \left(\hat{q}\theta^2\right)^{-1/3}\,. \tag{5}$$

Hence the line $t_{\mathrm{f}} = t_{\mathrm{d}}$ is parameterized by

$$\log z\theta = \frac{1}{3}\log\frac{1}{\theta} + \log\frac{\hat{q}^{1/3}}{p_{\mathrm{T}}}\,, \tag{6}$$

[2] In this discussion, we neglect the influence of rare, hard kicks in the medium that go beyond this definition.

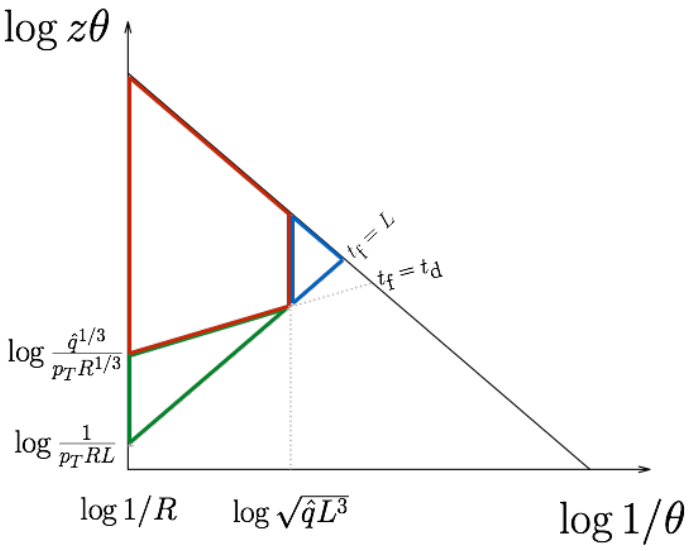

Figure 2: Lund diagram for vacuum radiation with inclusion of relevant medium scales related to creation and decoherence of partons in the medium. The parameters are $\hat{q} = 2$ GeV^2/fm, L = 2 fm and $p_T = 300$ GeV.

and the area above this line represents the phase space for vacuum emissions. As is clear from Figure 2, this guarantees that at angles smaller than the minimal decoherence angle $\theta_c \sim (\hat{q}L^3)^{-1/2}$, the decoherence time is automatically larger than the medium length.[3] In particular, emissions with $t_f < t_d < L$ correspond to pure vacuum splittings inside the medium that, during their subsequent propagation and possible further branching, will be resolved by medium interactions. Note also that the intersection point $t_f = t_d$ corresponds to emissions with a transverse momentum scale $Q_s \sim (\hat{q}L)^{1/2}$ and the characteristic energy $\omega_c \sim \hat{q}L^2$. The three time-scales we have identified – the formation time, t_f, the decoherence time, t_d, and the length of the medium, L – can be arranged in three possible orderings. These are marked out on Figure 2 as $t_f < t_d < L$ by the red area, $t_f < L < t_d$ by the blue area and $t_d < t_f < L$ by the green area, respectively. The second ordering is particularly interesting, giving rise to splittings that are formed inside the medium yet remain completely unresolved by medium interactions due to strong interference effects. It is often referred to as the coherence regime.

Before moving on, let us briefly contemplate a different model for the medium interactions. In this case, the resolution scale of the medium is simply the inverse of the medium momentum exchange, $\lambda_\perp \sim q_\perp^{-1}$. Now, the decoherence time is $t_d \sim (\theta q_\perp)^{-1}$ which gives to a minimal coherence angle $\theta_c \sim (q_\perp L)^{-1}$. In effect, the coherence regime exists only for sufficiently soft interactions $q_\perp < \sqrt{p_T/L}$.

Now let us briefly review the possible additional radiative channels that are opened due to interactions with the medium. It is important to stress that the emission probability for medium-induced radiation, such as Eq. (1) for the vacuum radiation, does not factorize in the same way. Hence, the phase space in the Lund diagram is not anymore uniformly filled.

Let us firstly describe the multiple scattering regime. It applies to situations when, in course of their formation, induced gluons experience transverse momentum broadening, approximated by $\langle k_\perp^2 \rangle \lesssim \hat{q}t_f$, see e.g. [19] for a more thorough discussion. We can invert this relation to find that the formation time of the emitted particles becomes $t_f(\omega) \sim \sqrt{\omega/\hat{q}}$. Gluons with the longest formation time $t_f = L$, carry energy $\omega_c \sim \hat{q}L^2$. This energy scale also acts as an effective cut-off scale, as for $\omega > \omega_c$ the spectrum is strongly suppressed (LPM suppression). It also determines a "minimal" angle for gluon emission due to multiple scattering, denoted $\theta_f(\omega_c) \sim (\hat{q}L^3)^{-1/2}$, that we already encountered as a minimal angle for coherence in the discussion above. It involves formation times longer than the decoherence time $t_f \gtrsim t_d$, which implies $k_f \lesssim \sqrt{\hat{q}\omega}$, and angles $\theta > \theta_c$. Furthermore, the multiplicity of LPM gluons becomes large in the soft sector, in particular at $\omega \lesssim \alpha_s^2 \omega_c$. In this regime, resummation of multiple medium-induced gluons is necessary.

This medium-induced radiative component is expected to enhance the yield around $t_f \sim t_d$. It is however worth keeping in mind that due to broadening and subsequent splitting, it is expected that these

[3] Since, $t_d > L$ doesn't make much sense physically, we have represented this element by a dashed line in Figure 2.

quanta will be effectively transported out of the jet cone. What remains is therefore a residual impact of "energy loss" that affects the vacuum like branchings inside the medium, see Section 2.3 for results from in-medium Monte Carlo showers.

In addition to the (relatively) soft emissions that are sensitive to multiple scattering, there arises a radiative component from rare, hard kicks in the medium. This component is formally higher-twist, i.e. scales as $\sim k_\perp^{-4}$, and has to be induced inside the medium, $t_\mathrm{f} < L$. It is however subleading to the the LPM emissions that dominate close to the line $t_\mathrm{f} \sim t_\mathrm{d}$. These emissions will typically not undergo further splittings and can contribute to the intra-jet distribution.

To summarize, from perturbative arguments regarding medium-induced radiative processes we expect to observe large medium-effects in the region marked by green in Figure 2, which overlaps with the region where LPM radiation is abundant. In the absence of medium interactions, the theoretical expectation is approximately reproduced by vacuum Monte Carlo showers, see Section 2.2 for more details. In Section 2.3 we compare our theoretical expectation with models that implement medium modifications. This concludes the physics discussion of possible radiative contributions at the level of single splitting. It is worth keeping in mind that what we have discussed so far is an idealized picture that will be complicated by the embedding the jets into correlated and un-correlated medium backgrounds. We have also neglected a set of other effects, such as medium back-reaction, that could possibly become important for realistic modeling of the jet-medium interactions.

2.2 Filling the map from reclustered of jets

The generalization of this picture to multiple emissions is more delicate. In vacuum, subsequent emissions are self-similar (apart from the running of α_s) which allows to iterate the splitting process with the jet opening angle R replaced by the splitting angle of the parent dipole (angular ordering) [17].

In order to connect theory with experimental observables, one relies on an operational definition of what a jet is. Such procedures cluster the final-state stable particles using sequential recombination algorithms, e.g. as implemented in FastJet [**?**, **?**]. Final state particles i and j are assigned a mutual distance d_{ij} and a distance to the beam $d_{i\mathrm{B}}$. The pair with the smallest distance are recombined first, and the algorithm repeats until the distance to the beam is the smallest quantity. In this case, the algorithm terminates labelling i a jet. The distance metric is generally defined as

$$d_{ij} = \min\left(p_{\mathrm{T},i}^{2\alpha}, p_{\mathrm{T},j}^{2\alpha}\right) \frac{\Delta R_{ij}^2}{R^2}\,, \tag{7}$$

$$d_{i\mathrm{B}} = p_{\mathrm{T},i}^{2\alpha}\,, \tag{8}$$

where $\Delta R_{ij}^2 = (\Delta\phi_{ij})^2 + (\Delta\eta_{ij})^2$ and α is a constant that defines the algortihm; $\Delta\phi_{ij}$ ($\Delta\eta_{ij}$) being the separation of the particles in azimuthal angle (pseudorapidity). In our studies, we have used the anti-k_T algorithm ($\alpha = -1$) [12], the Cambridge/Aachen (C/A) algorithm ($\alpha = 0$) [13, 14], and the k_T algorithm ($\alpha = 1$) [15, 16].

Given a reconstructed jet, obtained from a full heavy-ion event, with a list of constituents belonging to it one can repeat the recombination using one of the algorithms described above. In this context, this is referred to as a reclustering of the jet, providing a complete hierarchical tree (aka "history") of the jet evolution. Substructure techniques, to be used extensively throughout this report, define observables based on the information organized in such a tree. It is important to keep in mind that, depending on the reclustering algorithm, the information stored in the tree is only approximately related to the sequence of quark and gluon splittings that build the jet structure as understood within perturbative QCD.

In order to extract relevant information from a sample of real (simulated) jets, we apply the following procedure. For a given jet in the sample, fill the Lund diagram by

1) build a history of splittings by reclustering a jet with a given reclustering algorithm,

2) at each branching, extract the variables z and θ. Here, we define $z \equiv z_\mathrm{rel} = p_{t,j_2}/(p_{t,j_1} + p_{t,j_2})$ and use $\log(z\Delta R_{j_1 j_2}/R)$ as the quantity on the y-axis, where j_i ($i = 1, 2$) refer to two branches of the tree. This definition of z has the property that it always reflects the momentum sharing within that specific step.

The C/A reclustering, where the distance metric is only determined by the angular separation, see Eq. (7), should correspond most closely to a angular-ordered sequence of splittings based on our arguments above. That means that the last step of jet reclustering merges two substructures separated at large angles. Alternative reclustering strategies can however be used, although it would distort the correspondence

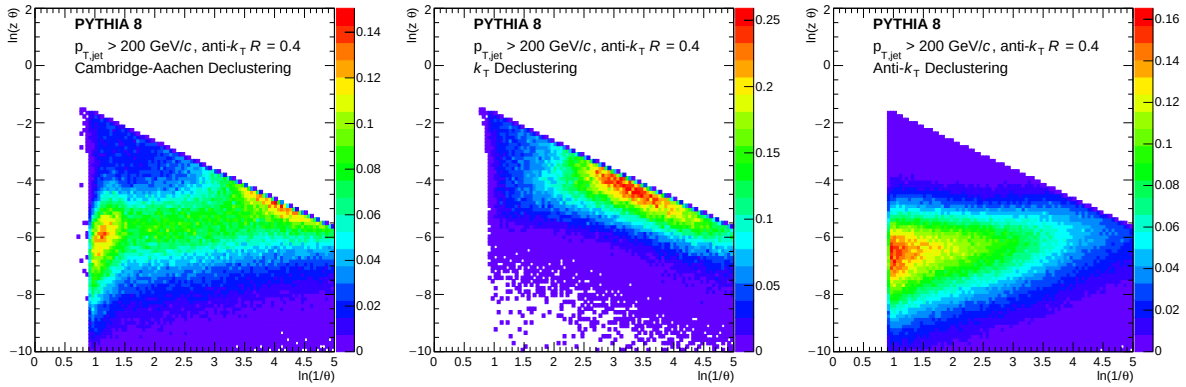

Figure 3: Lund diagrams reconstructed from a sample anti-$k_{\mathrm{T}} = 0.4$ jets generated by PYTHIA8. Three reclustering strategies were considered: C/A (left), k_{T}(middle), and anti-k_{T} (right).

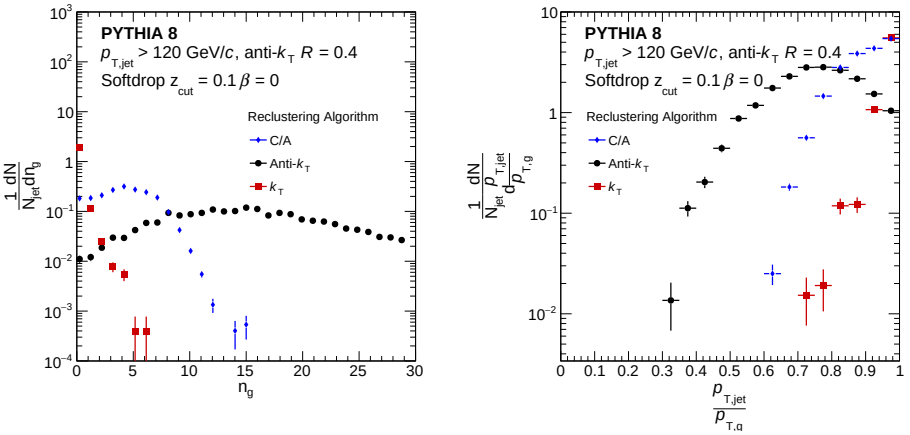

Figure 4: Effects of grooming on trees that are built up using different reclustering algorithms. Left plot: number of grooming steps. Right plot: ratio of jet p_{T} before and after grooming.

with showers that implement angular ordering. Given that we also will study other types of parton showers, e.g. that include medium effects, we have also studied the use of the (anti-)k_{T} algorithms in this step. In the case of the k_{T}-algorithm, the softest particles are clustered first. As a consequence, the last reclustering step will merge hard splittings. The anti-k_{T} clusters hard particles first, thus splittings at the last reclustering steps will be generally soft.

Using this procedure for the three different reclustering algorithms, we analyzed a sample of jet generated by PYTHIA in Figure 3. The jet sample corresponds to reconstructed anti-$k_{\mathrm{T}} = 0.4$ jets with $p_{\mathrm{T}} > 200$ GeV/c. The expected, simple features are nicely realized for the C/A reclustering, see Figure 3 (left). In particular, we see a slow enhancement of radiation at fixed $k_{\perp}$ which can mainly be attributed to running-coupling effects. The additional features can be attributed to effects from the underlying event that was not subtracted in this sample. Indeed, the maps generated by the (anti-)k_{T} reclustering are not uniform and possess and enhanced sensitivity to collinear, Figure 3 (center), and soft, large-angle configurations, Figure 3 (right), as naively expected.

The change of algorithm also strongly affects what happens to the jet after grooming. In Figure 4 (left), we show the distribution of the number of grooming steps for the three reconstruction algorithms discussed above. In particular, we note that the $k_{\perp}$ and the anti-$k_{\perp}$ algorithms result in completely different grooming. While the jet reconstructed with the former algorithm are mainly unaffected by grooming, in the latter case of the order of $\sim 10 - 20$ branches are groomed away. This also strongly affects the p_{T} of the groomed jet, as seen in Figure 4 (right), where the groomed jets in the anti-$k_{\perp}$ sample on average lose $\sim 20\%$ of their energy. The C/A algorithm falls in between the two extremes, as usual. Of the order of ~ 5 branches are removed by the grooming procedure on average, which slightly reduces

the jet p_{T} by $\lesssim 10\%$.

As pointed out before, medium-induced radiation does not per se follow the same (angular) ordering as described above. In fact, the resummation of soft radiation leads to quite different characteristics. We will however continue to apply the procedure outlined above to identify regions of particular medium modification in the following Section. Varying the reclustering algorithm can potentially enhance the sensitivity to different regimes, as found in the study above.

2.3 Radiation phase space and sensitivity to jet quenching

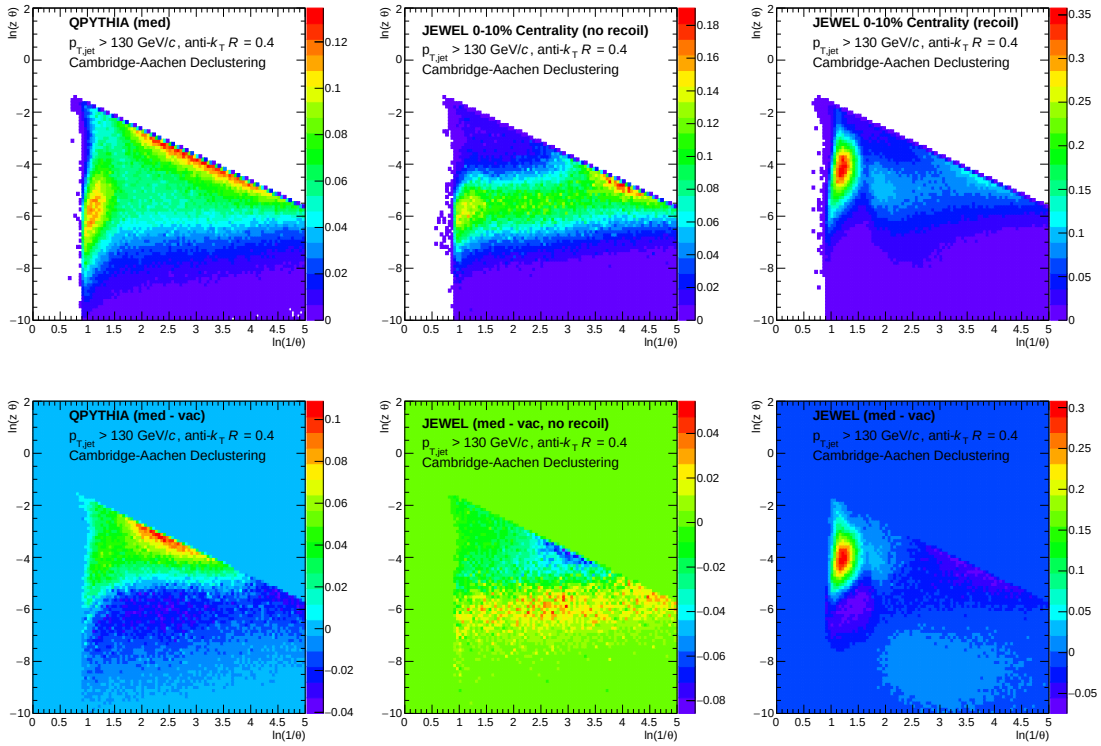

Figure 5: Lund diagram reconstructed from jets generated by QPYTHIA (left column), JEWEL without recoils (middle column) and JEWEL with recoils (right column). The lower panels correspond to the difference of the radiation pattern with and without jet quenching effects. Note that the scale of the z-axes varies between the panels.

As a demonstration of the general ideas outlined above, we fill the Lund diagram using two pQCD-based models for jet quenching, namely QPYTHIA [5] and JEWEL [6, 7]. Both models implement the possibility for medium-induced bremsstrahlung. The former model provides the possibility to track recoiling medium constituents that have interacted with the jet and, finally, include them in the hadronization step. Hence, the jet-induced medium response constitutes a correlated background that can contribute to the modifications of the measured jet substructure. In the opposite case, the model only contains an additional radiative component with respect to vacuum. Recoil effects are expected to contribute in the soft-large angle sector of the phase space, similarly to the uncorrelated underlying event, discussed further in Section 2.3.1. We refer to the two possibilities as "Recoil on" and "Recoil off". For further details regarding the models, see Appendix A.

For the same jet criteria as in Figure 3, in Figure 5 (upper row) we plot the Lund diagrams generated by QPYTHIA, JEWEL without recoils and JEWEL with recoils, respectively. In this particular study, we focus on the C/A reclustering. The lower plots show the differences to the corresponding vacuum diagrams. The results from QPYTHIA exhibit an modest excess $\sim 10\%$ of hard quanta relative to vacuum, see Figure 5 (lower, left). In the model, the number of splittings is increased relative to vacuum leading to a significant intra-jet momentum broadening. In the case of JEWEL, the difference plot does not show an increase of splittings but rather a small suppression $\sim 6\%$ of hard quanta, see Figure 5 (lower, center). This suppression is consistent with a lack of intra-jet broadening and a more collimated

fragmentation. This shows that the realistic modifications to the Lund diagram are highly non-trivial and calls for a better theoretical understanding, see Section 2.1 for a discussion. When the medium recoils are included, an excess of semi-hard and large angle quanta appears, see Figure 5 (lower, right). We note that in our declustering approach the angles are always measured relative to the hardest parent or subjet, in which case the angular distribution can be broader than the angular distribution measured relative to the jet axis that is used to compute jet profiles , see for instance [20].

It is worth pointing out that the medium-induced signal populates different regions of phase space in the two jet quenching models. While these features ultimately will be reflected in the relevant observables, the mapping onto the Lund kinematical plane seem to be a powerful tool to identify the impact of various medium modifications. Performing additional grooming, that is picking out branchings with specific properties, allows to enhance the sensitivity to the signal depending on the grooming parameters, see Section 3. Furthermore, changing the reclustering algorithm could also boost the signal, cf. Figure 3. We have seen that, in the case of JEWEL, the suppression of hard splittings is enhanced to $\sim 14\%$ with k_{T} reclustering. In the case of QPYTHIA, the excess of hard splittings is enhanced to $\sim 20\%$ with k_{T} reclustering.

The impact of the recoils as modeled by JEWEL has been extensively documented [20, 21]. Its contribution is needed to describe most of the jet shapes measured so far at the LHC. In particular, if the medium response can smear the subleading subjet momentum above the given grooming cut, the subjet momentum balance or z_g can become more asymmetric relative to vacuum. As a correlated background, the medium response cannot be experimentally subtracted to isolate purely radiative modifications to the jet shower. However, a cross-correlation of jet substructure observables might help to suppress its influence [21].

It is worth noting that, albeit in a complicated form, the splitting map contains of the information about a given medium shower. Certainly, such a procedure can be directly applied to experimental data, apart from the aspect of uncorrelated background that we outline in the next Section. Hence, in the remaining part of the report, the observables we choose to analyze will reflect particular features that already appear in the splitting map.

2.3.1 Sensitivity to uncorrelated background

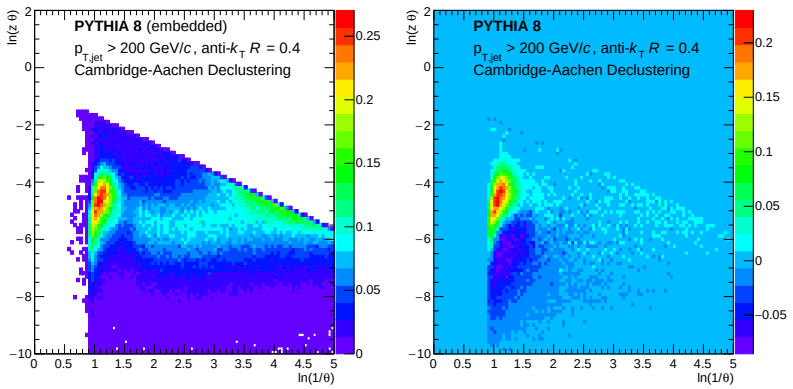

Figure 6: Impact of the uncorrelated background in the splitting map of the PYTHIA shower.

In all the studies performed so far in this Section, we have not included the effect of considering a realistic heavy-ion background. In these studies, we have been using thermal events corresponding to a momentum density of $\rho = 120$ GeV which corresponds to the most central events in the CMS detector, corresponding to a total multiplicity of ~ 7000 particles. More details on background, where do we take it from, parameters, referecens etc.. Details on embedding...

Hence, ending this section, we would also like to point out the fragility of using the Lund kinematical diagram in a realistic, noisy environment. The heavy ion background that is uncorrelated to the jet will populate the phase space in the form of soft splittings at large angle $\theta \sim R$, where the area is maximal. Depending on the considered jet p_T, these fake splittings can contribute significantly to the distribution of groomed observables, cf. Section 3, by enhancing the number of asymmetric splittings and inducing a strong modification relative to vacuum jets. Figure 6 shows the Lund diagram filled iteratively with

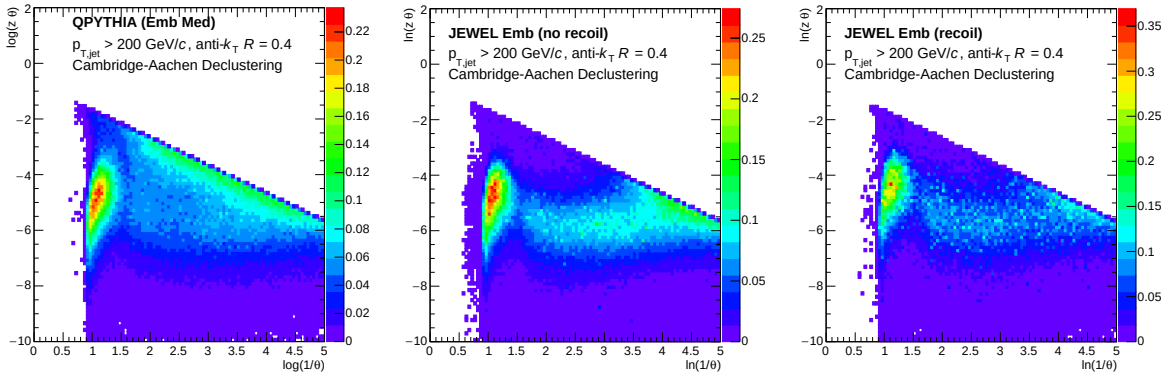

Figure 7: Impact of the uncorrelated background in the splitting map of the medium parton showers QPYTHIA and JEWEL. Upper row shows the resulting splitting map when embedding the modeled showers in a background.

PYTHIA jets embedded into a thermal background (left) and the difference plot to PYTHIA (right). The difference plot shows the enhancement of uncorrelated splittings at large angles. This provides a hint that, no matter the grooming settings, this becomes a significant contribution to the observable the smaller the p_{T}.

As expected, this a prominent feature for the in-medium showers as well. Similar plots are shown for QPYTHIA and JEWEL embedded showers are shown in Figure 7. The upper row correspond to QPYTHIA, JEWEL "Recoils Off" and JEWEL "Recoils on" embedded onto a thermal background. Strikingly, all three plots share a similar dominant feature at large angles. This is confirmed by subtracting the generator-level events from the embedded ones. However, we observe that after embedding, the difference to the vacuum reference (also embedded) is still significant, meaning that the differences in the fragmentation pattern from different generators survive the presence of an underlying event, albeit with significant distortions.

3 Jet substructure

As mentioned before, jet substructure techniques usually involve a step which reorganizes the constituents of a jet into a hierarchical tree where the nodes represent the splittings of sub-jets. This structure serves for subsequent analysis using additional techniques called jet grooming and tagging algorithms. Grooming techniques usually reorganizes the tree by discarding radiation that fail to pass given criteria, typically soft and large-angle radiation. Taggers, on the other hand, aim at identifying the first splitting that passes a given criterion. In this way it splits a jet into two sub-jets. There has been a lot of progress recently utilizing these techniques for a wide range of substructure observables [22, 23, 24, 25, 9], for a recent review see e.g. [26].

While jet fragmentation functions and other jet shape observables have been studied experimentally until recently these techniques had not been used in the context of heavy-ion collisions. Jet grooming was recently introduced as a tool to study the medium modification of leading partonic components in a parton shower [27], for related theoretical interpretations see [28, 29, 21, 30]. These subjets provide access to the properties of the first splitting of the parton evolution in the vacuum [31, 32].

Given the proliferation of existing techniques, we will only refer to these as grooming techniques and, in our studies, concretely study one, namely the Soft Drop procedure. The Soft Drop algorithm reclusters the anti-k_{T} jet constituents using C/A to create an angular-ordered clustering tree. On this tree a pairwise declustering is performed. In each step of the declustering the softer branch is removed until a branch is found that satisfies

$$\frac{\min(p_{\mathrm{T},i}, p_{\mathrm{T},j})}{p_{\mathrm{T},i} + p_{\mathrm{T},j}} > z_{\mathrm{cut}} \left(\frac{\Delta R_{ij}}{R_0}\right)^{\beta}, \tag{9}$$

where the subscripts "i" and "j" indicate the subjets at that step of the declustering, ΔR_{ij} is the distance between the two subjets, R_0 is the cone size of the anti-k_{T} jet, and z_{cut} and β are adjustable parameters. By varying z_{cut} and β specific regions of the emission phase space, see Figure 2, can be isolated. For

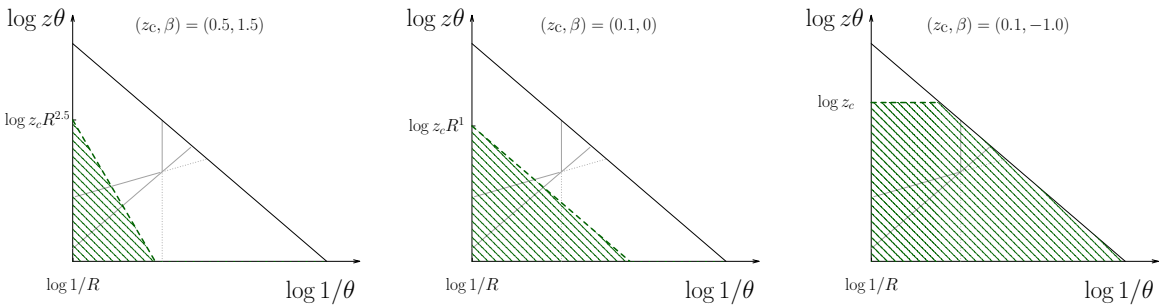

Figure 8: The three grooming settings studied in this report, see text for details, with the same medium scales as in Figure 2 (left). Shaded areas correspond to configuration that are groomed away.

$\beta = 0$, this procedure is identical to the modified mass-drop tagger [25]. It allows to design specific grooming settings sensitive for example semi-hard radiation from single hard scatterings, soft radiation in the BDMPS regime and soft contribution originating from heating up the medium while the parton shower traverses it.

We compare three grooming settings:

SD1: $z_{\rm cut} = 0.1$ and $\beta = 0$: this removes branches based on the momentum scale only;

SD2: $z_{\rm cut} = 0.5$ and $\beta = 1.5$: this has a stronger grooming at large angle;

SD3: $z_{\rm cut} = 0.1$ and $\beta = -1.0$: this setting selects only the hard radiation;

How these different settings cut into the emission phase space is shown Figure 8. While the first setting is the more widely used in various studies of the SD procedure, the two latter are designed to suppress regions of phase space with a lot of medium activity, as identified in the diagrams in Figure 5. One could, of course, devise other grooming strategies, or even combine various conditions, in order to "carve" out kinematical regimes of particular interest. We avoid such prescriptions here in order not to bias our sample excessively. On the other hand, it could be interesting to combine grooming strategies with specific reclustering algorithms, a point we briefly study in Section 3.1.1.

3.1 Groomed substructure observables and sensitivity to jet quenching

After identifying the first splitting that satisfies Eq. (9), we have access to the full kinematics of that branching process. The groomed jet-$p_{\rm T}$ is now defined as $p_{{\rm T}g} \equiv p_{{\rm T},1} + p_{{\rm T},2}$, where the subscripts now refer to the chosen sub-jets. We can then define the groomed momentum fraction, $z_g = \min\left(p_{{\rm T},1}, p_{{\rm T},2}\right)/p_{{\rm T}g}$ and the angle ΔR_{12}. In our numerical studies, we will focus on these two quantities but also introduce the groomed mass M_g, defined as in Eq. (2) with all relevant quantities being groomed. These observables shed light on how the branchings occur in course of the parton shower and are sensitive to medium effects as long as the branching originates from inside the medium, $t_{{\rm f}g} \equiv 2p_{{\rm T}g}/M_g^2 < L$. For the chosen medium parameters, the samples analyzed with settings SD1 and SD2 will contain an admixture of in-medium and out-of-medium splittings, see Figure 8, while SD3 picks exclusively out hard splittings originating from inside the medium.

As in the previous section, the jet quenching Monte Carlo event generators we use in our study are QPYTHIA and JEWEL (with recoil on and off) and are shown in Figure 9, 10 and 11. Jets were reconstructed using anti-$k_{\rm T} = 0.4$ and have $p_{\rm T} > 130$ GeV/c. The results in this section are obtained from generator level. In particular, we have not introduced any detector resolution effects, such as a minimal angular cut-off $\Delta R_{\rm min}$. Note, that the distributions are normalized by the total number of anti-$k_{\rm T}$ (ungroomed) jets. The distributions are therefore not self-normalized and contain information how grooming affects the overall suppression of the (groomed) jet yield.

Figure 9 shows the momentum fraction carried by the softest subjet for different event generators. The vacuum baseline is represented by the PYTHIA8 data points and compared to results from the QPYTHIA and JEWEL jet quenching event generators. The most striking feature is the generally opposite trend of the two models. This can also be traced back to the discussion around Figure 5. The modified parton shower in QPYTHIA makes the jets broader with respect to jets in vacuum and therefore many more

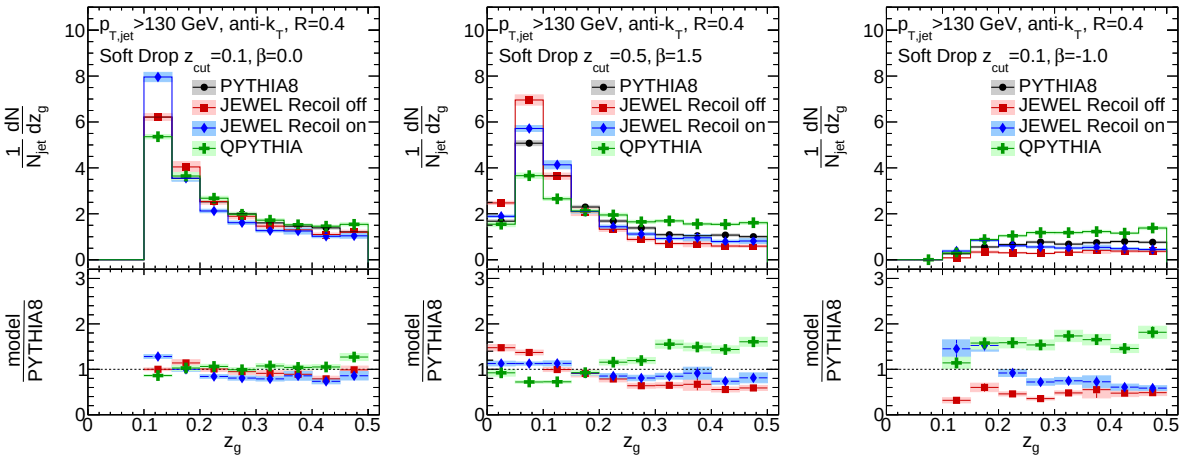

Figure 9: Groomed shared momentum fraction, z_{g}, for three different grooming settings in simulations with and without jet quenching. The uppers panels show the z_{g} distribution normalized by the total number of ungroomed jets while the lower panels show the ratio of JEWEL and QPYTHIA with respect to PYTHIA8.

jets survive the grooming. JEWEL however collimates the jets and therefore less jets are surviving the grooming with this setting.

We also note, that while for $\beta \geq 0$, see Figure 9 (left and center), the number of jets for the different generators remains roughly constant while for the negative grooming setting $\beta < 0$, Figure 9 (right), a large deviation from unity can be observed. Interestingly, QPYTHIA subjets are strongly enhanced in this regime while JEWEL subjets are strongly suppressed, both by a factor ~ 2.

Comparing the JEWEL results with and without recoil demonstrates that, for the chosen analysis settings, this observable is not very sensitive to recoil effects except for the the small-z_g region. In order to compare to the data presented in [27], see also [21] for a study using JEWEL, where a significant deviation from vacuum baseline was observed, we again point out that no minimal angular cut-off was employed in our studies. Such a cut-off suppresses collinear vacuum radiation and, hence, amplifies the effects related to the medium.

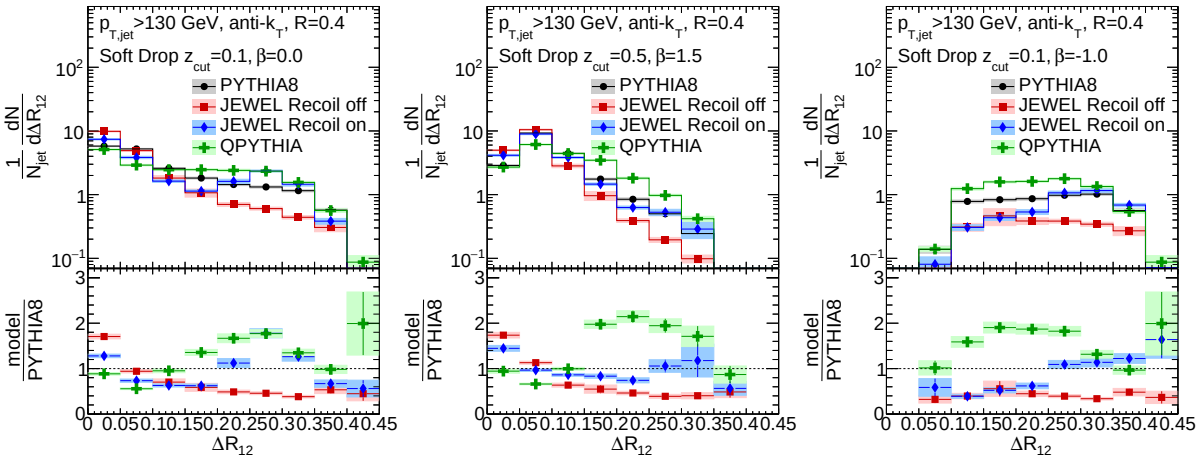

Figure 10: Distance between the two groomed subjets, ΔR_{12}, for three different grooming settings in simulations with and without jet quenching. The uppers panels show the ΔR_{12} distribution normalized by the total number of ungroomed jets while the lower panels show the ratio of JEWEL and QPYTHIA with respect to PYTHIA8.

Next we turn to studying the angular region where medium effects set in. One particularly interesting aspect is whether substructures are quenched according to their angular separation. The angular distance between the groomed sub-jets is plotted in Figure 10 for the three grooming settings. Once again, we see

big differences between the MC models; JEWEL being very collimated and QPYTHIA very broad. The effect in JEWEL primarily shows up at large angels for all explored grooming settings.

Finally, we study the groomed jet mass normalized by the transverse momentum, $M_{\mathrm{g}}/p_{\mathrm{T,jet}}$, in Figure 11. This observable combines the features already seen before.

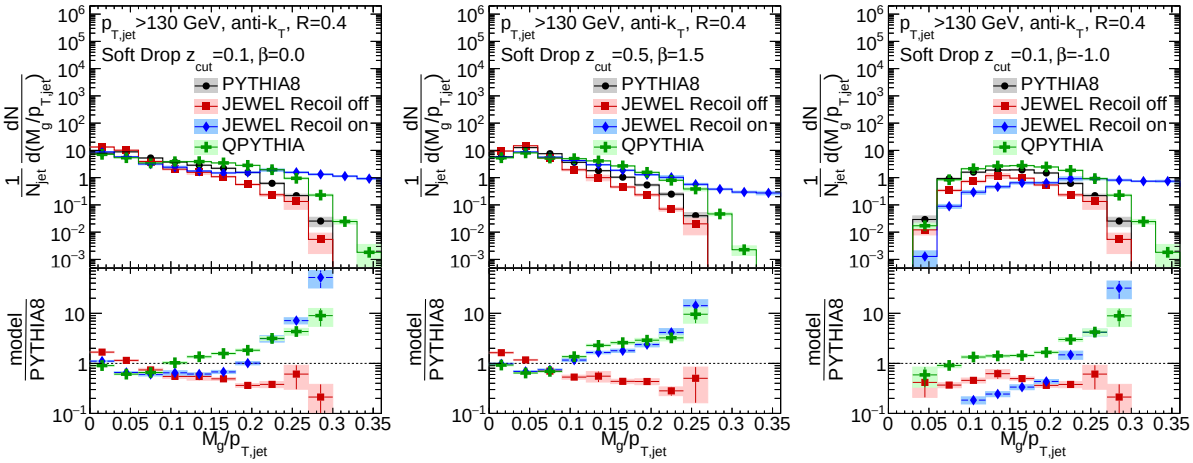

Figure 11: Groomed jet mass, $M_{\mathrm{g}}/p_{\mathrm{T,jet}}$, for three different grooming settings in simulations with and without jet quenching. The uppers panels show the $M_{\mathrm{g}}/p_{\mathrm{T,jet}}$ distribution normalized by the total number of ungroomed jets while the lower panels show the ratio of JEWEL and QPYTHIA with respect to PYTHIA8.

3.1.1 Sensitivity to hadronization and reclustering algorithm

The last stage of the jet fragmentation is the non-perturbative process of hadronization. This is a dynamical process that converts colored partons into color-singlet hadrons. In jet quenching event generators it is assumed that hadronization occurs outside of the medium. A proof for this assumption does not exist and therefore hadronization uncertainties should be expected to be sizable.

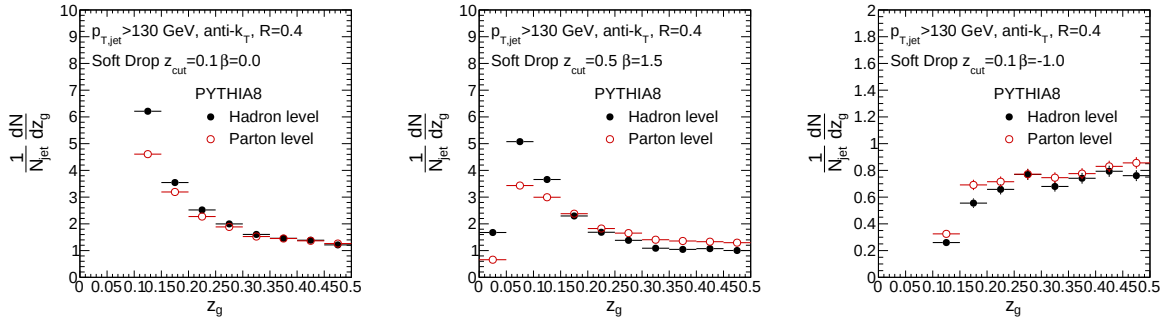

Figure 12: Groomed shared momentum fraction, z_{g}, for three different grooming settings in simulations with and without hadronization with the PYTHIA8 event generator.

Even for vacuum physics, it is well known that the SD procedure has some sensitivity to hadronization effects, for $\beta = 0$ see [33]. From perturbative arguments hadronization corrections to the jet p_T grow like R^{-1} [34] and so are potentially important for subjet observables. However, since hadronization is a process that happens locally in phase space, jets are less sensitive to the hadronization uncertainties than observables based on hadrons. In this paragraph we investigate how sensitive groomed subjet observables are to the hadronization process. For this purpose we compare the z_{g}-distribution in PYTHIA8 with and without hadronization for the three SD settings, described above, as shown in Figure 12. It can be observed that the low-z_{g} region is particularly sensitive to hadronization effects. For grooming with negative β the hadron- and parton-level results are most similar, see Fig, 12 (right), because with these grooming settings the soft splittings are rejected. Dedicated studies of these effects in conjunction with medium-modified hadronization are left for the future.

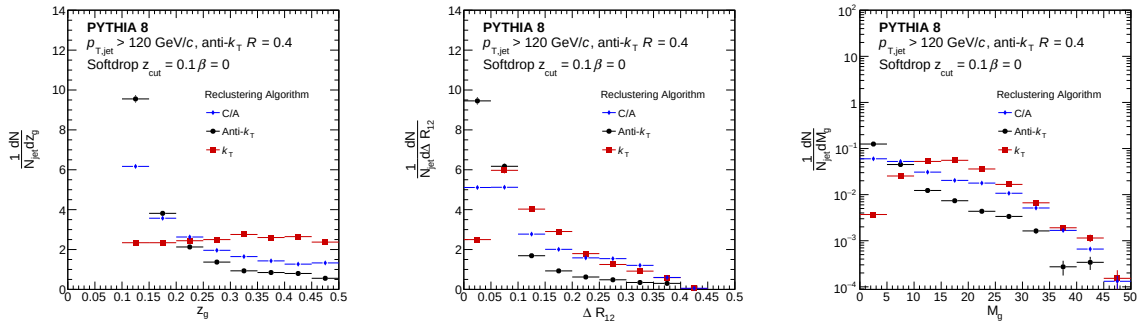

Figure 13: Subset of grooming variables, symmetry parameter (z_g), groomed mass (M_g) and groomed radius (ΔR_{12}) for three different jet reclustering algorithms.

Finally, we studied the behavior of the three observables subject to different reclustering algorithms applied, see Figure 13. In this particular case, we limit ourselves only to looking at the PYTHIA samples. In case of a grooming prescription that requires a semi-hard splitting, for instance like in the SD1 setting, the number of groomed branches will be large for anti-$k_{\rm T}$ reclustering ($\lesssim 30$) and very small for $k_{\rm T}$, for which the grooming conditions will be satisfied at the first iteration in most of the cases. Consistently, the groomed momentum fraction $z_{\rm g}$ probes very asymmetric splittings in the case of anti-$k_{\rm T}$ reclustering as can be seen in Figure 13 (left). In contrast, $k_{\rm T}$-reclustered $z_{\rm g}$ picks exclusively up symmetric splittings, resulting in an almost featureless distribution. Similar conclusions can be made for the ΔR_{12} distribution, Figure 13 (center), and M_g, Figure 13 (right), as well.

3.2 Unrolling/dissecting jet quenching observables using grooming

Many jet quenching observables, such as the nuclear modification factor R_{AA} and the momentum imbalance in photon-jet events, are considered benchmark measurements. However, their constraining power to discriminate between models have also been questioned. In some cases, the influence of background fluctuations can also obscure their constraining power.

In this section we present studies of conventional jet quenching observables that are enhanced by "unrolling" the jet samples using grooming techniques. As a first step, we apply SD grooming on the jet sample, extracting from each on the grooming variables z_g and ΔR_{12}. From these variables we can divide the sample in many ways. We have simply reorganized the fully inclusive sample according to the angle separating the two hardest prongs of a particular jet. This is motivated by the splitting maps and the results obtained for the substructure observables previously. Another motivation is to differentiate between the modifications of the "soft" and the "hard" structure of the jet. The former is more dominant for inclusive observables and for non-restrictive SD settings, e.g. SD1 and SD2 in Figure 8 (left and central panels), while the latter would be more pronounced for conservative SD parameter choices, such as SD3 in Figure 8 (right panel).

We have not attempted to study this in any systematic way. Here, we only report on two sample studies at LHC of the R_{AA} unrolled with SD1 and the $x_{J\gamma}$ distribution unrolled with SD2. More importantly, all results in this section have been computed by embedding the MC jet samples into a realistic heavy-ion background that depends on centrality. Hence they represent more realistically the magnitude of effects that should be expected to arise in heavy-ion collisions at the LHC.

The well-known nuclear modification factor, R_{AA}, is a standard benchmark for estimating/tuning medium parameters in jet quenching calculations. However, by dividing the sample of inclusive high-$p_{\rm T}$ jets into small- and large-angle configurations we gain access to more differential information regarding the accompanying modifications of the intra-jet structure. Similar studies, albeit using another method to dissect the jet sample into two-prong structures, was already presented in [**?**, **?**].

The jet samples generated from QPYTHIA, JEWEL "Recoil off" and JEWEL "Recoil on" that goes into calculating R_{AA} in Figure 14, has been divided using SD3 grooming into samples related to the angular separation of the hardest branches. While all three models gives a similar $p_{\rm T}$-trend of R_{AA} for the fully inclusive sample (see black points in Figure 14), large differences are seen for the unrolled results.[4] In QPYTHIA, the core of the jet is quenched stronger than the periphery, as expected from previous

[4] The overall magnitude of the inclusive R_{AA} does not play an important role for the point we are trying to make.

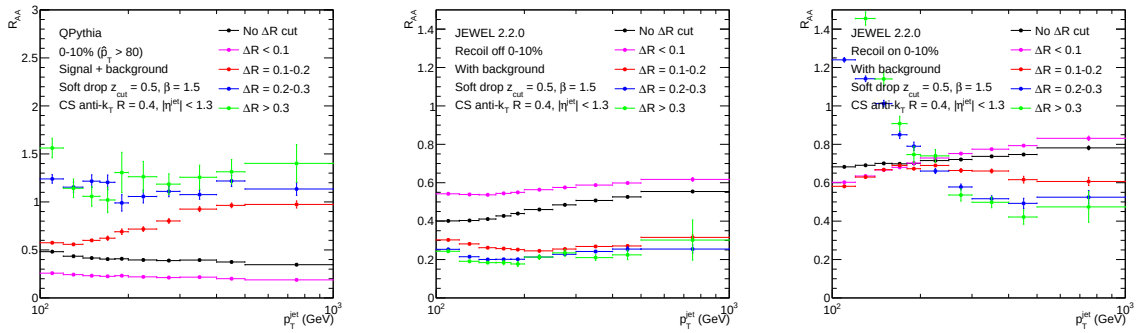

Figure 14: The nuclear modification factor for subsamples of jets that have been unrolled as a function of ΔR of the leading sub-jets identified using SD1.

studies above. For JEWEL(recoil-off), the effect is completely opposite: the jet core is quenched much less than large-angle splittings. This comes as no surprise in light of other substructure observables that were analyzed above, see e.g. Section 3.1. Including recoil effects, the JEWEL sample contains a strong p_{T}-dependence of large-angle jets and stands completely out. This could hint of an enhanced sensitivity to medium recoil in this observable.

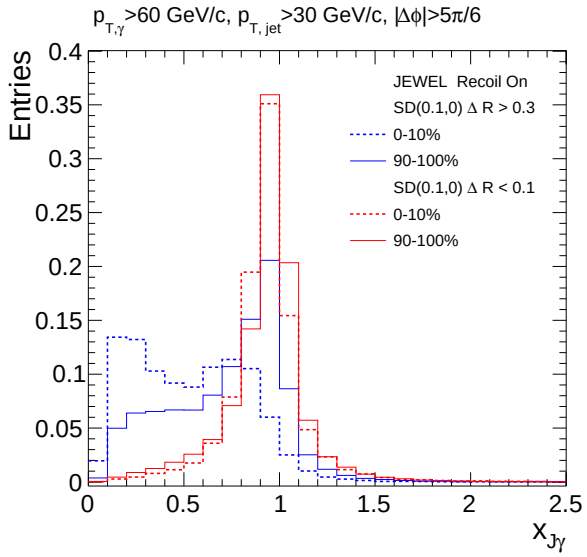

Figure 15: The $x_{J\gamma}$ distribution for subsamples of jets that have been unrolled as a function of the angle found between the leading sub-jets using SD.

Another benchmark observable is the photon-jet momentum asymmetry. We recall that the variable $x_{J\gamma}$ is defined as the ration of jet to photon momentum, $x_{J\gamma} \equiv p_{\perp,\mathrm{jet}}/p_{\perp,\gamma}$. In Figure 15 we have only included results for JEWEL with recoils turned on. Again, this sample has been unrolled as described above, this time using SD2 grooming. The same features that have been pointed out multiple times, also show up here as a function of collision centrality. Notable, the small-angle sample shows very little dependence of centrality, and is closely peaked around 1. The large-angle sample, on the other hand, is already very different in vacuum (i.e. the 90-100% curve in Figure 15) and evolves significantly from central to peripheral.

These proof-of-point studies illustrate the enhanced sensitivity to more than one variable one obtains by unrolling the underlying jet sample using a well-controlled procedure. However, the results shown in this section are only exploratory and more systematic studies are left for the future.

4 Outlook

The investigation of QCD jet observables in heavy-ion collisions is a community-wise effort, involving both experimentalists and theorists. While significant progress, both from the point of view of the development of experimental techniques as well as from theoretically founded parametric estimates grounded on scale analysis and modeling within Monte-Carlo parton showers, has led to a quite detailed qualitative *general* understanding of how jets are modified in the medium created in the aftermath of heavy-ion collisions, the field has not reached the level of precision associated with jet measurements in other colliding systems, such as proton-proton and DIS. It is therefore worth considering whether it be possible and fruitful to contemplate strategies that would be useful to further enhance jet observables as unique and valuable probes of the quark-gluon plasma. A first attempt at such an ambitious step would be to find a common language within the field of heavy-ions for comparisons between experimental data and theory. However, it is almost as important to develop common ground with the wider field of high-energy physics, based on the language of perturbative QCD and the tools of modern high-energy experiments.

The "Novel tools and observables for jet physics in heavy-ion collisions" workshop provided an opportunity to work toward this goal. The concrete calculations and model studies presented in this report can, of course, be further scrutinized and improved. However, the main messages could be relevant for the field at large. Let us summarize in two points.

- We have introduced a operational way to map the full content of a jet splitting process, making use of the Lund diagram. Using kinematical arguments, we can make sense of enriched and depleted regions of phase space as results of medium interactions and recoil. An important caveat is that this idealized picture gets strongly distorted due to the presence of uncorrelated background but we have shown, through various exercises, that this aspect mostly affects the low-p_{T} observables.

- We have outlined a strategy to single out jet samples enriched in configurations possessing specific properties as an aid to single out physics mechanisms, in particular *hard* (e.g. medium-induced bremsstrahlung, modifications of intra-jet structure due to energy loss) from *soft* (e.g. particle yield, sensitivity to recoil) medium effects and, similarly, *large-angle* from *small-angle* components.

We hope the topics we have reported here would trigger new and exciting future studies of jet, and in particular jet substructure, observables in heavy-ion collisions.

Acknowledgements

We thank the CERN TH department for hosting and supporting the organization of the 5th Heavy Ion Workshop and the TH institute "Novel tools and observables for jet physics in heavy-ion collisions" and especially Michelangelo Mangano and Angela Ricci for providing organizational support before and during the meeting. M.S. was supported by Grant Agency of the Czech Republic (18-12859Y). J.G.M.'s work was supported by the Fundação para a Ciência e Tecnologia (Portugal) under contracts CERN/FIS-NUC/0049/2015, CERN/FIS-PAR/0022/2017, and Investigador FCT - Development Grant IF/00563/2012. DVP acknowledges funding from the Department of Energy under award DE-SC0018117. LA was supported by Fundação para a Ciência e Tecnologia (FCT, Portugal) under contracts CERN/FIS-NUC/0049/2015 and SFRH/BPD/103196/2014. HAA acknowledges support from the Science and Technology Facilities Council (https://stfc.ukri.org/). CB was supported in part by Swedish Research Council, contracts number 2012-02283 and 2017-0034.

A Monte-Carlo parton showers

This section briefly outlines the main physics ingredients of the MC in-medium parton shower generators used in course of the workshop. For detailed descriptions, we refer the interested reader to the original references.

A.1 QPYTHIA

This appendix provides some details of the implementation of medium effects on the final-state parton shower as implemented in QPYTHIA [5]. As the name suggests, the program builds on PYTHIA6 [4, **?**].

The final-state shower is a mass-ordered (or virtuality-ordered) shower, where the Sudakov form factor is defined as

$$\Delta(t_1, t_0) = \exp\left[\int_{t_0}^{t_1} \frac{\mathrm{d}t}{t} \int_{z_-}^{z^+} \mathrm{d}z \, \frac{\alpha_s(t)}{2\pi} P(z)\right] , \tag{10}$$

where the limits $z_\pm = z_\pm(t)$ implements the perturbative constraints and the evolution variable $t = M^2$ is the (squared)virtuality or invariant mass, see Eq. (2). The quantity in Eq. (10) represents the probability of no splitting between the mass-scales t_0 and t_1 and can be used to determine the variables (z, t) of the subsequent splitting in the shower by a standard dicing procedure. Although the shower is ordered in mass, angular ordering is enforced by a veto procedure.

In vacuum, the function $P(z)$ corresponds to the relevant Altarelli-Parisi splitting functions. However, in the medium one takes advantage of the fact that the medium-induced radiative spectrum comes simply in addition to the existing vacuum one [**?**, **?**], to substitute

$$P(z) \to P^{\mathrm{tot}}(z) = P(z) + \Delta P(z) \tag{11}$$

in Eq. (10), where

$$\Delta P(z) = \frac{2\pi t}{\alpha_s} \frac{\mathrm{d}I^{\mathrm{med}}}{\mathrm{d}z\mathrm{d}t} , \tag{12}$$

where $\mathrm{d}I^{\mathrm{med}}/(\mathrm{d}z\mathrm{d}t)$ is identified with the (double-differential) BDMPS spectrum. In the current implementation of QPYTHIA it is computed in the multiple-soft scattering approximation, that neglects hard medium interactions, and in the soft limit $z \ll 1$. In addition, the splitting function $g \to q\bar{q}$ is not modified by this prescription since it is subleading.

A.2 JEWEL

JEWEL is also based on PYTHIA6, and handles exclusively the final-state parton shower routine. Let us summarize the main steps of the modified shower routine in three points.

- Within the program, every interaction with the medium is treated similarly to the hard, partonic scattering itself and described by a $2 \to 2$ perturbative matrix element, suitably regularized in the IR due to the dressing of medium quasi-particles. Hence, one invokes so-called "partonic parton densities" to allow hard medium kicks to resolve additional (virtual) jet constituents in course of the interaction. Scattering with the medium can also give rise to additional radiation.

- The emission with the shortest formation time is realized first. This allows for a smooth interpolation between so-called vacuum emissions and the ones that are affected by medium interactions, often referred to as "medium-induced".

- The LPM effect carefully implemented by keeping track of the amount of re-scattering during the formation time of radiation.

Comparing to the analytical limits of single-gluon radiation spectrum, this treatment allows to treat the kinematics of emission and the interactions on a more precise level.

In addition to the showering, JEWEL also permits to track the momenta and color flow of the recoiling medium constituents that happen to interact with the jet. Note that the medium parton is counted as a final-state particle directly after the scattering, and is not allowed to interact further. We refer to this mode as "Recoils on". The mode "Recoils off" refer to the case when these partons are not included in the event record and discarded. In the former case, it is imperative to subtract the thermal momentum of the partons before their interaction with the jet, since it forms part of the uncorrelated thermal background in heavy-ion events. This is most reliably done with the so-called "4MomSub" procedure which consists of subtracting the sum momenta of medium constituents entering a given jet, for further details see [20].

References

[1] N. Armesto, et al., Comparison of Jet Quenching Formalisms for a Quark-Gluon Plasma 'Brick', Phys. Rev. C86 (2012) 064904. arXiv:1106.1106, doi:10.1103/PhysRevC.86.064904.

[2] K. M. Burke, et al., Extracting the jet transport coefficient from jet quenching in high-energy heavy-ion collisions, Phys. Rev. C90 (1) (2014) 014909. arXiv:1312.5003, doi:10.1103/PhysRevC.90.014909.

[3] CERN TH Institute "Novel tools and observables for jet physics in heavy-ion collisions"/5th Heavy Ion Jet Workshop (2017).
URL https://indico.cern.ch/event/625585/

[4] T. Sjostrand, S. Mrenna, P. Z. Skands, A Brief Introduction to PYTHIA 8.1, Comput. Phys. Commun. 178 (2008) 852–867. arXiv:0710.3820, doi:10.1016/j.cpc.2008.01.036.

[5] N. Armesto, L. Cunqueiro, C. A. Salgado, Q-PYTHIA: A Medium-modified implementation of final state radiation, Eur. Phys. J. C63 (2009) 679–690. arXiv:0907.1014, doi:10.1140/epjc/s10052-009-1133-9.

[6] K. C. Zapp, J. Stachel, U. A. Wiedemann, A local Monte Carlo framework for coherent QCD parton energy loss, JHEP 07 (2011) 118. arXiv:1103.6252, doi:10.1007/JHEP07(2011)118.

[7] K. C. Zapp, F. Krauss, U. A. Wiedemann, A perturbative framework for jet quenching, JHEP 03 (2013) 080. arXiv:1212.1599, doi:10.1007/JHEP03(2013)080.

[8] B. Andersson, G. Gustafson, L. Lonnblad, U. Pettersson, Coherence Effects in Deep Inelastic Scattering, Z. Phys. C43 (1989) 625. doi:10.1007/BF01550942.

[9] A. J. Larkoski, S. Marzani, G. Soyez, J. Thaler, Soft drop, JHEP 05 (2014) 146. arXiv:1402.2657, doi:10.1007/JHEP05(2014)146.

[10] P. Berta, M. Spousta, D. W. Miller, R. Leitner, Particle-level pileup subtraction for jets and jet shapes, JHEP 06 (2014) 092. arXiv:1403.3108, doi:10.1007/JHEP06(2014)092.

[11] M. Cacciari, G. P. Salam, G. Soyez, SoftKiller, a particle-level pileup removal method, Eur. Phys. J. C75 (2) (2015) 59. arXiv:1407.0408, doi:10.1140/epjc/s10052-015-3267-2.

[12] M. Cacciari, G. P. Salam, G. Soyez, The Anti-k(t) jet clustering algorithm, JHEP 04 (2008) 063. arXiv:0802.1189, doi:10.1088/1126-6708/2008/04/063.

[13] Y. L. Dokshitzer, G. D. Leder, S. Moretti, B. R. Webber, Better jet clustering algorithms, JHEP 08 (1997) 001. arXiv:hep-ph/9707323, doi:10.1088/1126-6708/1997/08/001.

[14] M. Wobisch, T. Wengler, Hadronization corrections to jet cross-sections in deep inelastic scattering, in: Monte Carlo generators for HERA physics. Proceedings, Workshop, Hamburg, Germany, 1998-1999, 1998, pp. 270–279. arXiv:hep-ph/9907280.
URL http://inspirehep.net/record/484872/files/arXiv:hep-ph_9907280.pdf

[15] S. Catani, Y. L. Dokshitzer, M. H. Seymour, B. R. Webber, Longitudinally invariant K_t clustering algorithms for hadron hadron collisions, Nucl. Phys. B406 (1993) 187–224. doi:10.1016/0550-3213(93)90166-M.

[16] S. D. Ellis, D. E. Soper, Successive combination jet algorithm for hadron collisions, Phys. Rev. D48 (1993) 3160–3166. arXiv:hep-ph/9305266, doi:10.1103/PhysRevD.48.3160.

[17] Y. L. Dokshitzer, V. A. Khoze, A. H. Mueller, S. I. Troian, Basics of perturbative QCD, 1991.

[18] R. K. Ellis, W. J. Stirling, B. R. Webber, QCD and collider physics, Camb. Monogr. Part. Phys. Nucl. Phys. Cosmol. 8 (1996) 1–435.

[19] A. Kurkela, U. A. Wiedemann, Picturing perturbative parton cascades in QCD matter, Phys. Lett. B740 (2015) 172–178. arXiv:1407.0293, doi:10.1016/j.physletb.2014.11.054.

[20] R. Kunnawalkam Elayavalli, K. C. Zapp, Medium response in JEWEL and its impact on jet shape observables in heavy ion collisions, JHEP 07 (2017) 141. arXiv:1707.01539, doi:10.1007/JHEP07(2017)141.

[21] J. G. Milhano, U. A. Wiedemann, K. C. Zapp, Sensitivity of jet substructure to jet-induced medium responsearXiv:1707.04142.

[22] J. M. Butterworth, A. R. Davison, M. Rubin, G. P. Salam, Jet substructure as a new Higgs search channel at the LHC, Phys. Rev. Lett. 100 (2008) 242001. arXiv:0802.2470, doi:10.1103/PhysRevLett.100.242001.

[23] S. D. Ellis, C. K. Vermilion, J. R. Walsh, Recombination algorithms and jet substructure: Pruning as a tool for heavy particle searches, Phys. Rev. D 81 (2010) 094023. arXiv:0912.0033, doi:10.1103/PhysRevD.81.094023.

[24] D. Krohn, J. Thaler, L.-T. Wang, Jet trimming, JHEP 02 (2010) 084. arXiv:0912.1342, doi:10.1007/JHEP02(2010)084.

[25] M. Dasgupta, A. Fregoso, S. Marzani, G. P. Salam, Towards an understanding of jet substructure, JHEP 09 (2013) 029. arXiv:1307.0007, doi:10.1007/JHEP09(2013)029.

[26] A. J. Larkoski, I. Moult, B. Nachman, Jet Substructure at the Large Hadron Collider: A Review of Recent Advances in Theory and Machine Learningarxiv:1709.04464.

[27] A. M. Sirunyan, et al., Measurement of the splitting function in pp and PbPb collisions at $\sqrt{s_{\mathrm{NN}}} =$ 5.02 TeVarXiv:1708.09429.

[28] Y.-T. Chien, I. Vitev, Probing the Hardest Branching within Jets in Heavy-Ion Collisions, Phys. Rev. Lett. 119 (11) (2017) 112301. arXiv:1608.07283, doi:10.1103/PhysRevLett.119.112301.

[29] Y. Mehtar-Tani, K. Tywoniuk, Groomed jets in heavy-ion collisions: sensitivity to medium-induced bremsstrahlung, JHEP 04 (2017) 125. arXiv:1610.08930, doi:10.1007/JHEP04(2017)125.

[30] N.-B. Chang, S. Cao, G.-Y. Qin, Probing medium-induced jet splitting and energy loss in heavy-ion collisionsarXiv:1707.03767.

[31] G. Altarelli, G. Parisi, Asymptotic freedom in parton language, Nucl. Phys. B 126 (1977) 298. doi:10.1016/0550-3213(77)90384-4.

[32] A. J. Larkoski, S. Marzani, J. Thaler, Sudakov Safety in Perturbative QCD, Phys. Rev. D 91 (2015) 111501. arXiv:1502.01719, doi:10.1103/PhysRevD.91.111501.

[33] M. Dasgupta, A. Powling, A. Siodmok, On jet substructure methods for signal jets, JHEP 08 (2015) 079. arXiv:1503.01088, doi:10.1007/JHEP08(2015)079.

[34] M. Dasgupta, L. Magnea, G. P. Salam, Non-perturbative QCD effects in jets at hadron colliders, JHEP 02 (2008) 055. arXiv:0712.3014, doi:10.1088/1126-6708/2008/02/055.